Synthesis, molecular structures and electrochemical investigations of [FeFe]-hydrogenase biomimics $[Fe_2(CO)_{6-n}(EPh_3)_n(\mu\text{-edt})]$ (E = P, As, Sb; n = 1, 2)

Shishir Ghosh[a,b,c], Ahibur Rahaman[b], Georgia Orton[c], Gregory Gregori[a], Martin Bernat[a], Ummey Kulsume[b], Nathan Hollingsworth[a], Katherine B. Holt[a], Shariff E. Kabir[b] and Graeme Hogarth[c*]

[a] *Department of Chemistry, University College London, 20 Gordon Street, London, WC1H 0AJ, U.K*

[b] *Department of Chemistry, Jahangirnagar University, Savar, Dhaka-1342, Bangladesh*

[c] *Department of Chemistry, King's College London, Britannia House, 7 Trinity Street, London SE1 1DB, UK*

Key Topics: Hydrogenase biomimics, hydrogen evolution reaction

Abstract: A series of ethane-dithiolate (edt = $S(CH_2)_2S$) complexes $[Fe_2(CO)_5(EPh_3)(\mu\text{-edt})]$ and $[Fe_2(CO)_4(EPh_3)_2(\mu\text{-edt})]$ (E = P, As, Sb), biomimics of the core of [FeFe]-hydrogenases, have been prepared and structurally characterised. The introduced ligand(s) occupies apical sites lying *trans* to the iron-iron bond. NMR studies reveal that while in the mono-substituted complexes the $Fe(CO)_3$ moiety undergoes facile trigonal rotation, the $Fe(CO)_2(PPh_3)$ centres do not rotate on the NMR timescale. The reductive chemistry has been examined by cyclic voltammetry both in the presence and absence of CO and the observed behavior is found to be dependent upon the nature of the substituents. With L = CO or $SbPh_3$ potential inversion is seen leading to a two-electron reduction, while for others (L = PPh_3, $AsPh_3$) a quasi-reversible one-electron reduction is observed. Protonation studies reveal that $[Fe_2(CO)_5(PPh_3)(\mu\text{-edt})]$ is only partially protonated by excess $HBF_4.Et_2O$, thus ruling complexes $[Fe_2(CO)_5(EPh_3)(\mu\text{-edt})(\mu\text{-H})]^+$ out as a catalytic intermediates, but $[Fe_2(CO)_4(PPh_3)_2(\mu\text{-edt})]$ reacts readily with $HBF_4.Et_2O$ to produce $[Fe_2(CO)_4(PPh_3)_2(\mu\text{-edt})(\mu\text{-H})]^+$. While all new complexes are catalysts for the reduction of protons in MeCN, their poor stability and relatively high reduction potentials does not make them attractive in this respect.

Keywords: hydrogenase, biomimic, pnictide, substitution, trigonal rotation

Introduction

Since the structural elucidation of the active site of [FeFe]-hydrogenases [**1-2**] biomimetics of this enzyme have attracted enormous attention, with a bewildering array of variants being prepared and studied as electrocatalysts for proton-reduction [**3-14**]. Since the enzymes contain a three-atom dithiolate bridge, the vast majority of studies have focused on propane-dithiolate (pdt = $S(CH_2)_3S$) and amine-substituted (adt = $SCH_2N(R)CH_2S$) dithiolate complexes, while in contrast, catalytic studies on the seemingly similar ethane-dithiolate (edt = $S(CH_2)_2S$) complexes as proton-reduction catalysts are more limited.

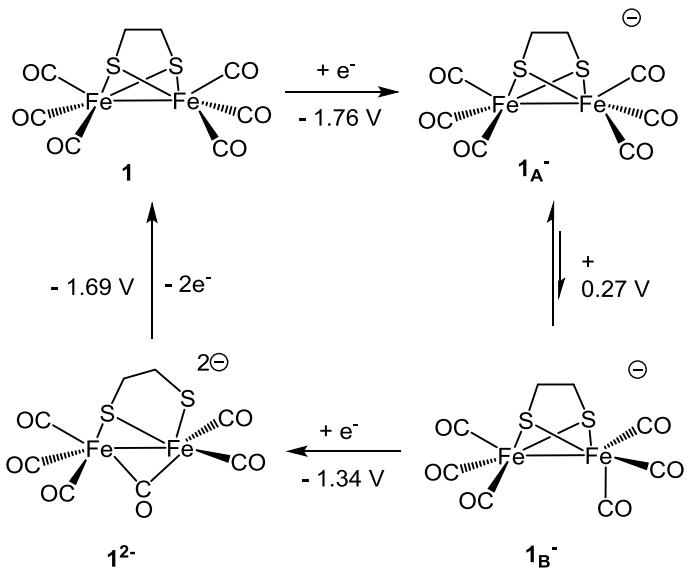

Scheme 1 Calculated potential inversion upon reduction of **1**

While edt- and pdt-bridged complexes have broadly similar chemical and physical properties, closer inspection reveals some important differences. For example while $[Fe_2(CO)_6(\mu\text{-edt})]$ (**1**) and $[Fe_2(CO)_6(\mu\text{-pdt})]$ (**1***) are reduced at a similar potential to generate a 35-electron radical anion, secondary transformations lead to the formation of tetrairon complexes resulting from either CO loss (edt) [**15**] or CO transfer (pdt) [**16**]. For **1**, dimerisation is suppressed under a CO atmosphere and Evans and co-workers noted a scan rate dependency on the number of electrons taken up, ranging smoothly between 1-2, with slower scan rates leading to potential inversion and the uptake of two-electrons [**17,18**]. In contrast the pdt analogue, **1***, shows no such potential inversion and is limited to the uptake of *ca.* one-electron except at very slow scan rates [**19**]. Density functional theory (DFT) calculations suggest that potential inversion in **1** results from a series of transformations as shown in

Scheme 1 (with calculated potentials) [**17**]. The initially generated (at -1.76 V) anion $\mathbf{1_A^-}$ can undergo a facile trigonal rotation to give the so-called rotated isomer, $\mathbf{1_B^-}$. The latter has a calculated reduction potential of –1.34 V, thus allowing addition of a second electron (potential inversion) with formation of a bridging carbonyl and concomitant cleavage of an iron-sulfur bond to give $\mathbf{1^{2-}}$. Thus the key chemical process which results in potential inversion is the trigonal rotation of an $Fe(CO)_3$ group and for **1** an activation barrier of ca. 51 kJ mol^{-1} has been measured by VT NMR studies [**20**].

While both **1** and **1*** can act as proton-reduction catalysts [**21-23**], they are not basic enough to bind a proton except by very strong acids [**24**] and thus reduction is the primary catalytic process. A common strategy in the development of functional [FeFe]-hydrogenase biomimics is the substitution of one or more carbonyl by stronger electron-donating ligands; increasing the basicity of the diiron centre and making it more susceptible to protonation. For triarylphosphines, substitution is favoured at an apical site (*trans* to the Fe-Fe vector) and, while increasing the basicity of the diiron centre, it also substantially increases the energy barrier for trigonal rotation at the substituted site, such that this process is no longer accessible. While there are many examples of phosphine-substituted hydrogenase biomimics, in contrast related substitution chemistry of the heavier group 15 elements have not been studied, the only related example we can find in the literature being $[Fe_2(CO)_5(AsPh_3)(\mu\text{-}SMe)_2]$ [**25**]. Herein we report the synthesis and structural characterisation of a series of **1** derivatives $[Fe_2(CO)_5(EPh_3)(\mu\text{-edt})]$ (**2-4**) and $[Fe_2(CO)_4(EPh_3)_2(\mu\text{-edt})]$ (**4-7**) (E = P, As, Sb) together with studies of their reductive chemistry as followed by cyclic voltammetry under both CO and argon atmospheres.

Results and discussion

Synthesis and characterisation. Mono-substituted $[Fe_2(CO)_5L(\mu\text{-edt})]$ (**2-4**; L = PPh_3, $AsPh_3$, $SbPh_3$) were prepared as shown in Scheme 2. For the phosphine adduct 2 we found that simply refluxing **1** and PPh_3 afforded the desired product, but for EPh_3 derivatives **3-4** a more effective preparation involved use of $Me_3NO.2H_2O$ in MeCN as a CO-removal agent. Disubstituted $[Fe_2(CO)_4L_2(\mu\text{–edt})]$ (**5-7**; L = PPh_3, $AsPh_3$, $SbPh_3$) were prepared upon heating MeCN solutions of **1** with a five-fold excess of the respective ligands and $Me_3NO.2H_2O$. Complex **5** was independently reported while this work was in progress [**26**].

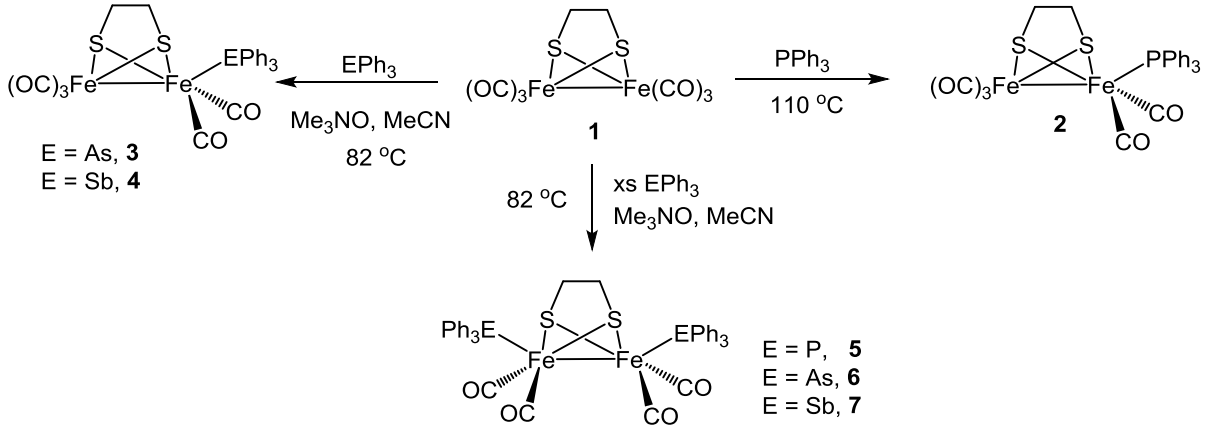

Scheme 2 Synthesis of **2-7**

All were isolated in good yields as air-stable red crystalline solids and are readily characterised on the basis of their IR spectra. For mono-substituted complexes, the highest frequency ν(CO) band for the edt complexes is consistently 3 cm^{-1} higher in energy than the analogous pdt complex, suggesting that the edt is slightly less electron-donating than pdt. Within each sub-group there is a small increase in the frequency of this band upon descending the group; **2** 2048 cm^{-1} < **3** 2050 cm^{-1} < **4** 2051 cm^{-1}. For disubstituted complexes **5-7** the highest frequency ν(CO) band was observed at 1999 cm^{-1} for all three complexes. ^{1}H NMR spectra of mono-substituted **2-4** show two different methylene environments; for **2** these appear as a pair of A_2B_2X multiplets centered at δ 1.92 and 1.21 in CD_2Cl_2 at room temperature. Lowering the temperature results in a slight broadening of each resonance but at all temperatures there was no evidence of a second isomer in solution. Similarly, the $^{31}P\{^{1}H\}$ NMR spectrum of **2** consists of a sharp singlet at all accessible temperatures, appearing at 62.9 ppm in CD_2Cl_2 at room temperature. This shows that in solution they consist of a single isomer. For disubstituted **5-7** the methylene protons are equivalent in the ^{1}H NMR spectrum and the $^{31}P\{^{1}H\}$ NMR spectrum of $[Fe_2(CO)_4(PPh_3)_2(\mu\text{–edt})]$ (**5**) consists of a singlet at all accessible temperatures, being observed at 61.3 ppm at room temperature in $CDCl_3$.

Structural studies. Molecular structures of **2-4** and **5-7** are shown in Figures 1-2 respectively and structural parameters, together with those for **1** [**27,28**] and **2*** [**29**], are summarised in Table 1. The mono-substituted phosphine and arsine complexes are isostructural (monoclinic $P2_1/c$), while the antimony analogue crystallises in the triclinic $P\bar{1}$ group but is structurally

very similar. Disubstituted **5-7** are isostructural (monoclinic $P2_1/n$). Iron-iron bond lengths are within expected limits spanning a small range between 2.4741(4)-2.5107(4) Å, the shortest in $[Fe_2(CO)_4(SbPh_3)_2(\mu\text{–edt})]$ (**7**) and the longest $[Fe_2(CO)_5(PPh_3)(\mu\text{–edt})]$ (**2**). This suggests there is no significant *trans*-influence. For comparison the Fe-Fe bond length in the two polymorphs of **1** are; $P2_1/n$ 2.505(2) Å [**30**] and $P\bar{1}$ 2.502(1) Å (-80 ^oC) and 2.497(4) Å (25 ^oC) [**27,28**]. All Fe-Fe distances are slightly shorter than found in $[Fe_2(CO)_4(PPh_3)_2(\mu\text{–pdt})]$ (**5***) [Fe-Fe 2.5167(16) Å] [**31**] and this slight shortening appears to be a general feature of edt- *vs* pdt-bridged complexes, which Pickett has related to the strength of the Fe-Fe bond [**32**]. Iron-sulfur bond lengths and angles are unexceptional and cover a small range. Iron-element bond lengths as expected increase by *ca.* 0.1 Å upon going down the group, and the Fe-As and Fe-Sb bond lengths of *ca.* 2.33 and 2.47 Å respectively. The most notable feature of all structures is the apical coordination of the introduced ligand(s) which lie approximately *trans* to the iron-iron bond [Fe-Fe-E 151.74(2)–158.10(2)^o]. In crystallographically characterised complexes of the type $[Fe_2(CO)_5(PAr_3)(\mu\text{-dithiolate})]$ [**31,33**] and $[Fe_2(CO)_4(PAr_3)_2(\mu\text{-dithiolate})]$ [**26,34**] the phosphine(s) occupy apical sites. In $[Fe_2(CO)_4(PPh_3)(PMe_3)(\mu\text{-edt})]$ [**35**] the PPh_3 also occupies an apical position, but the PMe_3 is in a basal site.

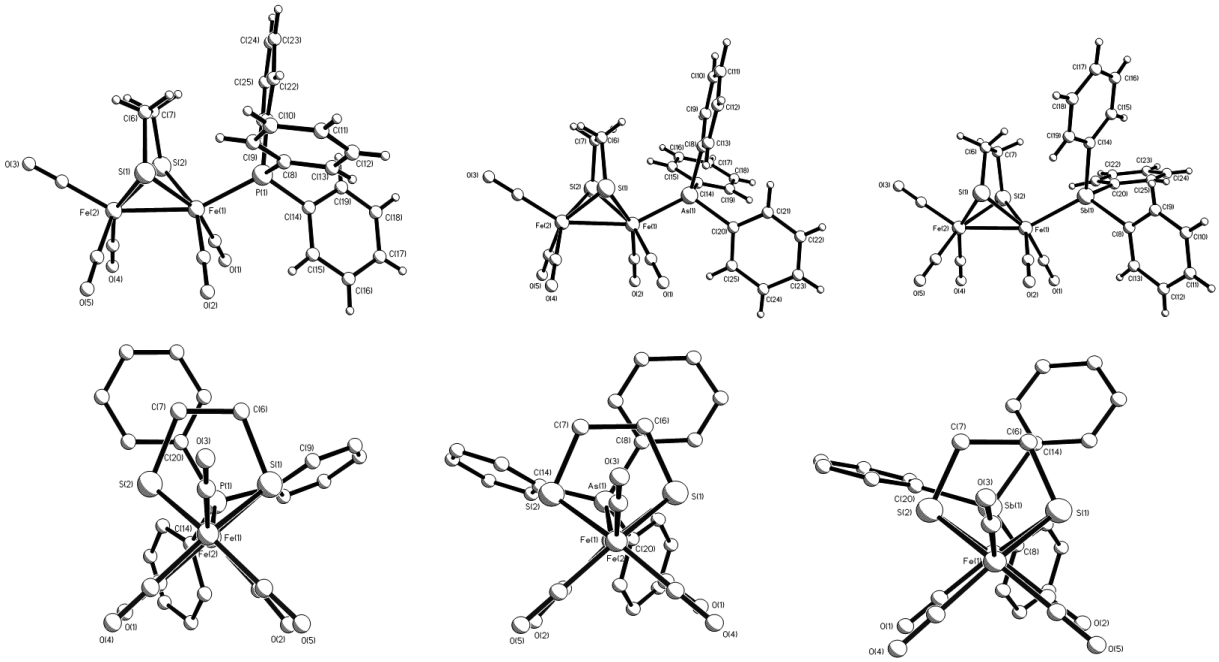

Figure 1. Molecular structures of $[Fe_2(CO)_5(PPh_3)(\mu\text{–edt})]$ (**2**), $[Fe_2(CO)_5(AsPh_3)(\mu\text{–edt})]$ (**3**) and $[Fe_2(CO)_5(SbPh_3)(\mu\text{–edt})]$ (**4**).

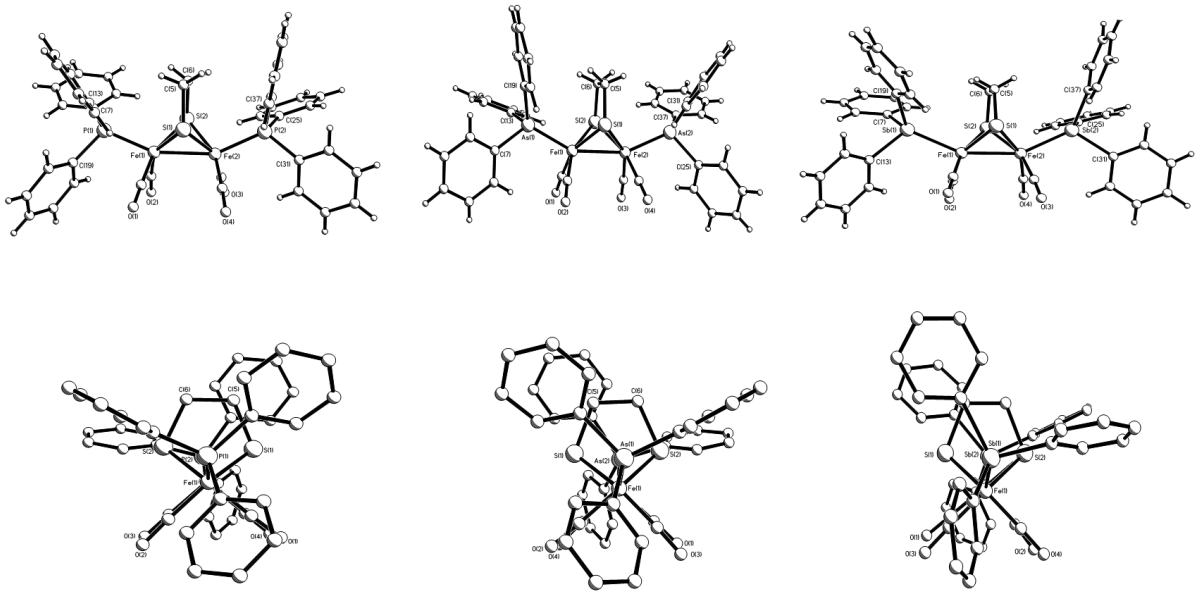

Figure 2. Molecular structures of $[Fe_2(CO)_4(PPh_3)_2(\mu\text{–edt})]$ (**5**), $[Fe_2(CO)_4(AsPh_3)_2(\mu\text{–edt})]$ (**6**) and $[Fe_2(CO)_4(SbPh_3)_2(\mu\text{–edt})]$ (**7**).

Trigonal rotation fluxionality. An important aspect of the reduction chemistry of **1** proposed by Felton *et al.* (Scheme 1) [**17**] is the trigonal rotation of an $Fe(CO)_3$ moiety upon reduction which then allows formation of a bridging carbonyl. It is not possible to probe this directly in the reduced form due both to the limited stability of the anion and also its paramagnetic nature. Consequently we probed the fluxionality of the $Fe(CO)_3$ sub-unit in **2** making the assumption that reduction would not significantly affect this (see below). For comparison, Darensbourg and co-workers have previously shown that $Fe(CO)_3$ trigonal rotation occurs in both **1** and **1*** is facile although free energies of activation vary significantly at ca. 51 and 35-36 kJ mol^{-1} respectively, as estimated from VT $^{13}C\{^1H\}$ NMR measurements [**36**]. The low-field region of the room temperature $^{13}C\{^1H\}$ NMR spectrum of **2** in CD_2Cl_2 shows a doublet at 215.2 ppm (J_{PC} 13.5 Hz) attributed to the equivalent pair of basal carbonyls on the substituted iron centre and a broad singlet at 210.4 ppm for the $Fe(CO)_3$ group, the carbonyls of which are interconverting rapidly on the NMR timescale. Upon cooling to 233 K, no significant change was observed for the low-field carbonyl doublet, but the higher field signal split into two separate singlet resonances at 212.7 and 206.5 in a 2:1 ratio. From these studies (T_c = 278 K, $\Delta\nu$ = 625 Hz) we estimate a free energy of activation of 44.5 ± 2 kJ mol^{-1} for the trigonal rotation in **2**. This is in accord with the value obtained for **1** and suggests that phosphine substitution, while completely changing the nature

of the fluxionality at the substituted iron atom, has relatively little impact upon the trigonal rotation of the $Fe(CO)_3$ group. Related experiments with **3** and **4** gave free energies of activation of 46.3 ± 2 and 44.5 ± 2 kJ mol^{-1} showing that while $Fe(CO)_3$ trigonal rotation in **2-4** is slightly lower in energy than in **1,** there is little effect upon changing the group 15 element. For disubstituted $[Fe_2(CO)_4(PPh_3)_2(\mu\text{–edt})]$ (**5**), the carbonyl region of the $^{13}C\{^1H\}$ NMR spectrum did not vary with temperature showing that trigonal rotation of $Fe(CO)_2L$ groups has a high energy barrier.

Protonation studies. Extensive protonation studies have been carried out on a range of hydrogenase biomimics [**32, 36-38**] with bridging hydrides almost always being observed. We have carried out a protonation studies on **2-7**. Addition of excess $HBF_4.Et_2O$ to a CH_2Cl_2 solution of **2** resulted in a slight lightening of the solution and the slow formation (over *ca.* 4 h) of a new product characterised by IR bands at 2110s, 2064s, 2053sh, 2021m and 2018m cm^{-1}. Reactions with **3** and **4** also led to the similar changes in the IR spectra, however, spectral changes were not so clean and some decomposition was apparent. Thus, as all appear to behave in the same way, we focused later studies on **2**. Addition of *ca.* 5 equivalents of $HBF_4.Et_2O$ to a CD_2Cl_2 solution of **2** resulted in a slight lightening of the red solution and both ^1H and $^{31}P\{^1H\}$ NMR spectra showed the formation of a small amount (*ca.* 5%) of a new complex characterised by a high-field doublet at δ -17.6 (J_{PH} = 2.2 Hz) in accord with formation of the bridging hydride $[Fe_2(CO)_5(PPh_3)(\mu\text{-edt})(\mu\text{-H})][BF_4]$ (**$2H^+$ap**). After a short time (ca. 5 min) a second hydride resonance appeared at δ -16.8 (J_{PH} = 20.0 Hz) and after 10 min the two hydride resonances were of approximately equal intensity. As coupling between apical phosphines and bridging hydrides is often small [**32**] and on the basis of the larger J_{PH} coupling constant we assign this second species to **$2H^+$ba** (Scheme 3). After 4 h the ratio of the two hydrides was still approximately equal but after longer periods (20 h) only **$2H^+$ba** was present. Unfortunately, these later spectra were broad, indicative of formation of either a paramagnetic species and/or decomposition. At all times the major resonance (*ca*. 90%) in the $^{31}P\{^1H\}$ NMR spectrum was that of **2**, but a later times (20 h) a singlet at 5.9 ppm characteristic of free PPh_3 was also observed. We rationalize these observations as shown in Scheme 3. The Fe_2 in **2** is not very basic and only at low pH are there detectable amounts of cationic hydrides. The initially formed **$2H^+$ap** rearranges via a trigonal twist of the $Fe(CO)_2(PPh_3)$ moiety to give **$2H^+$ba** characterised by the relatively large J_{PH} value. Formation of two isomers of **$2H^+$** was unexpected as isomerisation requires a trigonal twist

which we have shown is a high energy process. However it is not unprecedented and we not that Rauchfuss has recently reported that protonation of $[Fe_2(CO)_4(PPh_3)_2(\mu\text{-}S_2)]$ affords a mixture of isomers with apical-apical and apical-basal arrangement of the PPh_3 ligands [**26b**]. Thus while the trigonal twist is slow on the NMR timescale it is accessible on the synthesis timescale and $\mathbf{2H^+_{ap}}$ must be the thermodynamic product. Nevertheless, for the purposes of electrocatalytic studies (see below), at all acid concentrations only small amounts of $[Fe_2(CO)_5(EPh_3)(\mu\text{-}H)(\mu\text{-edt})]^+$ will be present, thus the predominant electrocatalytic process must be initiated by reduction.

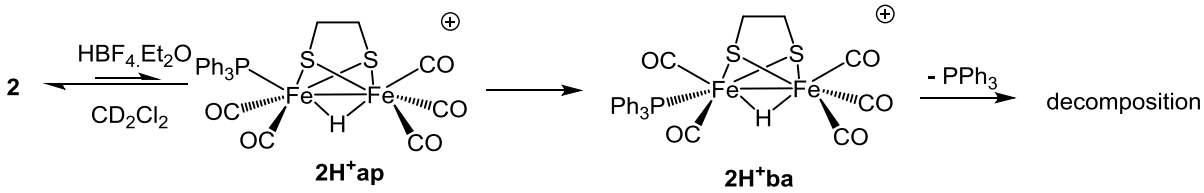

Scheme 3 Protonation of **2** by $HBF_4.Et_2O$

Addition of a slight excess of $HBF_4.Et_2O$ to a CH_2Cl_2 solution of **5** resulted in the slow formation of a new species characterised by ν(CO) resonances at 2060vs, 2040m and 2000s cm^{-1}; the shift of *ca.* 60 cm^{-1} to higher wavenumbers being consistent with formation of $[Fe_2(CO)_4(PPh_3)_2(\mu\text{-}H)(\mu\text{-edt})][BF_4]$ (**5H$^+$**). Related experiments with **6-7** showed similar changes and solutions of these cations were relatively stable over a period of hours. Low temperature ^1H NMR studies (-20 ^oC) showed that addition of $HBF_4.Et_2O$ to a solution of **5** in CD_2Cl_2 resulted in appearance of a singlet at δ -17.1 ppm. Pickett and co-workers have studied the protonation chemistry of $[Fe_2(CO)_4(PMe_3)_2(\mu\text{-edt})]$ (**8**) and $[Fe_2(CO)_4(PMe_3)_2(\mu\text{-pdt})]$ (**8***) in detail [**32**]. Both exist as a mixture of apical-apical and apical-basal isomers. They found that the rate of protonation of **8** was ca. 10 times slower than that of **8*** and also that protonation of **8** was more complicated than that of **8***, affording four spectroscopically characterised isomers of $[Fe_2(CO)_4(PMe_3)_2(\mu\text{-edt})(\mu\text{-H})]^+$ (**8H$^+$**). In only one of these, the apical-apical isomer, does the hydride appear as a singlet. This isomer is present immediately after protonation being generated from apical-apical **8** and on this basis the product of protonation of **5** is characterised as the apical-apical isomer $[Fe_2(CO)_4(PPh_3)_2(\mu\text{-}H)(\mu\text{-edt})][BF_4]$ (**5H$^+$**) (Scheme 4). Unlike the protonation of **2**, we did not observe any further changes upon standing. This is likely due to the high rotational barrier of the $Fe(CO)_2(PPh_3)$ groups which precludes secondary rearrangements observed for the PMe_3 analogue **8**. The

basicity of the diiron centers in **5** and **8** can be measured (to some extent) by the relative positions of their ν(CO) bands in the IR spectrum; the highest frequency bands appearing at 1999 and 1982 cm^{-1} respectively, highlighting the significantly more basic nature of the PMe_3-substituted center. Thus, in the presence of strong acids the major species present in solution for these disubstituted complexes is the protonated apical-apical isomer.

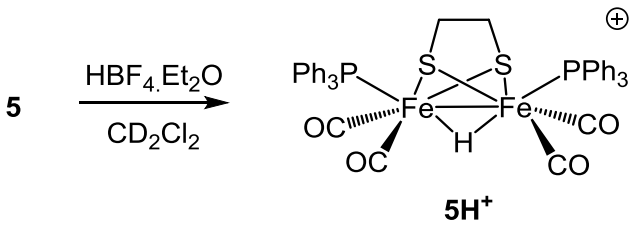

Scheme 4 Protonation of **5** with HBF_4

Electrochemistry. Cyclic voltammetry (CV) of **1-4** were carried out in CO or argon-saturated MeCN/0.1 M $TBAPF_6$ solutions over scan rates 10 mV s^{-1} to 10 V s^{-1}. The product of the one electron reduction in each case is the 35 electron anion, from which rapid loss of CO results in a more stable 33-electron product. Hence in argon-saturated solution the reduction of all complexes is irreversible over all scan rates (Fig. S1). In CO-saturated electrolyte CO ligand loss is suppressed, allowing for study of further reduction of the anion formed in the first electron transfer step. Figure 3 shows the normalised CVs for the four complexes in CO-saturated electrolyte at slow (20 mV s^{-1}) and fast (5 V s^{-1}) scan rates. Normalisation was carried out by dividing currents by the square root of the scan rate (Table 3).

Figure 3a shows similar behavior for **1** as noted previously by Best [**15**] and Evans [**17**]. At all scan rates reduction takes place at -1.75 V vs. Fc/Fc^+ however normalised peak current varies from 8.5 x 10^{-5} A $V^{-1/2}$ $s^{1/2}$ at 20 mV s^{-1}, consistent with a two electron reduction, to 4 x 10^{-5} A $V^{-1/2}$ $s^{1/2}$ at 5 V s^{-1}, which is tending towards a one electron reduction. Reduction appears reversible at slow scan rates, with an oxidation peak at -1.63 V and i_{ox}/i_{red} = 0.8. At the high scan rate there are two oxidation peaks, one at -1.63 V and the other at -1.2 V. These results are consistent with a potential inversion mechanism, as described by Felton *et al* [**17**]. In a CO atmosphere at slow scan rate, the trigonal rotation described in Scheme 1 takes place on the electrochemical timescale, allowing uptake of a second electron at the same or less negative potential. At faster scan rates there is insufficient time for the structural

change to take place, hence the reduction remains a one-electron process, as indicated by the smaller normalised reduction current. The one-electron reduction appears to be somewhat reversible, as indicated by the oxidation peak at -1.63 V. However, the magnitude of this peak is smaller than the reduction peak and taken with the additional oxidation peak at -1.2 V suggests some lack of stability of the anion.

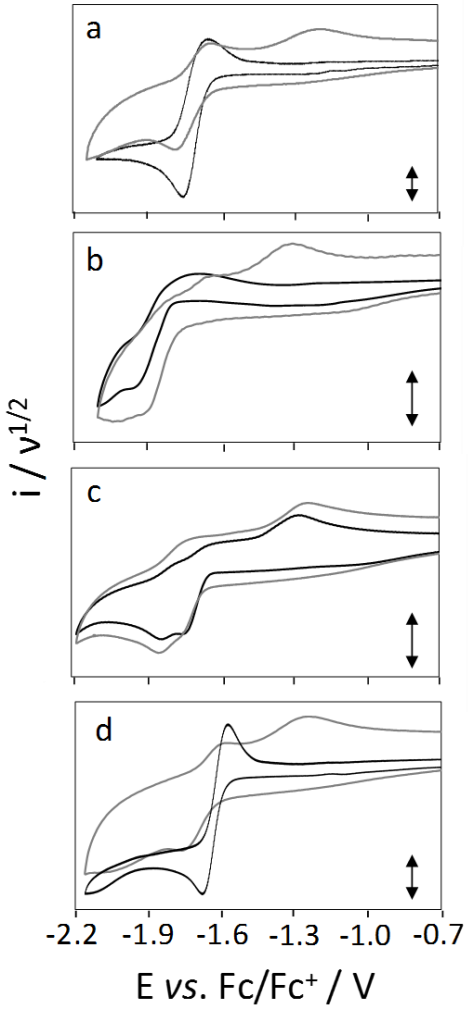

Figure 3 Normalised CVs at 20 mV s^{-1} (black) and 5 V s^{-1} (grey) for 0.5 mM complex in CO-saturated 0.1 M $TBAPF_6$ / MeCN: a) **1**; b) **2**; c) **3** and d) **4**. Vertical double headed arrows indicate normalised current of 20 µA $V^{-1/2}$ $s^{1/2}$ for each set of CVs.

Figures 3b-d show the effect of substitution on the redox properties of **1-4**. The potential at which the complex undergoes reduction is influenced by the substituting ligand, with the more σ-donating PPh_3 resulting in E_{red} at -1.9 V (at 5 V s^{-1}) for **2** [**39**]. In contrast reduction takes place at less negative potentials for **3** and **4** (ca. -1.75 V at 5 V s^{-1}). The $SbPh_3$ complex (Figure 3d) is the only one which shows a similar response to **1** and exhibits potential inversion. At slow scan rates a reversible electron transfer is observed, with normalised peak

currents tending towards a two electron process, while at faster rates a one-electron reduction followed by two oxidation peaks at different potentials is noted, exactly as observed for **1**. In contrast, reduction of **2-3** (Fig 3b-c) is mainly irreversible and the normalised reduction current remains constant over all scan rates. This suggests a different reduction mechanism is taking place and that there is no potential inversion for these complexes. In both cases the reduction peak consists of two overlapping responses and the normalised peak current is consistent with a process of between one and two electrons. The overlapping response suggests an initial one-electron reduction is followed by further reduction of the anion or a decomposition product at more negative potentials. The difference between this mechanism and the potential inversion mechanism is that any structural change taking place upon the first reduction step does not lead to facilitated uptake of a second electron at the same or less negative potential. All of the complexes exhibit an oxidation peak at a similar potential at fast scan rates (**1**, **3** and **4** at -1.2 V; **2** at -1.4 V) suggesting it can be attributed to oxidation of a similar species in each case, probably a product of the structural rearrangement or decomposition of the anion. Exhaustive electrolysis of edt complexes is reported to result in dimer formation [**15**], hence the oxidation peak may be attributed to such a species. The more negative potential for the oxidation peak in the case of **2** suggests the responsible species is PPh_3 substituted.

The electrochemical reduction response of the disubstituted complexes **5-7** were also investigated under argon and CO atmospheres. All showed a single reduction peak at more negative potentials than their mono-substituted counterparts: **5** -2.18 V; **6** -1.92 V and **7** -1.79 V. Normalised peak currents for their reduction was found to be independent of scan rate in all cases, indicating that potential inversion did not take place. The absence of potential inversion for **7** (Fig. S2) as compared to **4** in a CO atmosphere demonstrates that in **4** the rotation of the $Fe(CO)_3$ unit rather than $FeSb(CO)_2$ results in the structural rearrangement, consistent with the NMR results and calculations.

Complexes **2-7** all undergo oxidation (in MeCN), the potential of which changes substantially upon increasing the electron-density on the diiron centre (Figs. S4-5). Thus successive replacement of CO for PPh_3 leads to a decrease in oxidation potential by *ca*. 0.4 V per substitution, with similar reductions being observed for the heavier homologues. Unexpectedly for **2-4**, oxidation decreased slightly with increasing molecular weight, while for **5-7** oxidation potentials are (within experimental error) the same. The stability of the

oxidation product also varied significantly. Thus, while oxidation of both **1** and **2** is totally irreversible, oxidation of **5** shows good reversibility in both argon and CO. Oxidation of **6-7** was again irreversible, and in each case a second smaller oxidation wave at *ca.* + 0.25 V was observed.

Proton-reduction catalysis. Both **1** and **1*** have been shown to catalyse the reduction of protons to hydrogen at their first reduction potential and mechanisms have been probed [**40-42**]. Chiang and co-workers have prepared $[Fe_2(CO)_6(\mu\text{-H})(\mu\text{-edt})]^+$ (**1H**$^+$) from reaction of $[H(SiEt_3)_2][B(C_6F_5)_4]$ with **1**, and from **1H**$^+$ generated and spectroscopically characterised catalytic intermediates $[Fe_2(CO)_6(\mu\text{-H})(\mu\text{-edt})]$ (**1H**), $[Fe_2(CO)_5(\mu\text{-CO})(\mu\text{-H})(\mu\text{-edt})]^-$ (**1H**$^-$), $[Fe_2(CO)_5(\mu\text{-CO})(\mu\text{-H})(\mu\text{-edtH})]$ (**1-2H$_A$**) and $[HFe_2(CO)_5(\mu\text{-CO})(\mu\text{-H})(\mu\text{-edtH})]$ (**1-3H$_A$**$^+$). On the basis of these observations and detailed DFT calculations [**40-42**] it has proved possible to elucidate likely mechanistic pathways [**42**], a (somewhat abridged) mechanistic scheme for **1** being shown in Scheme 5.

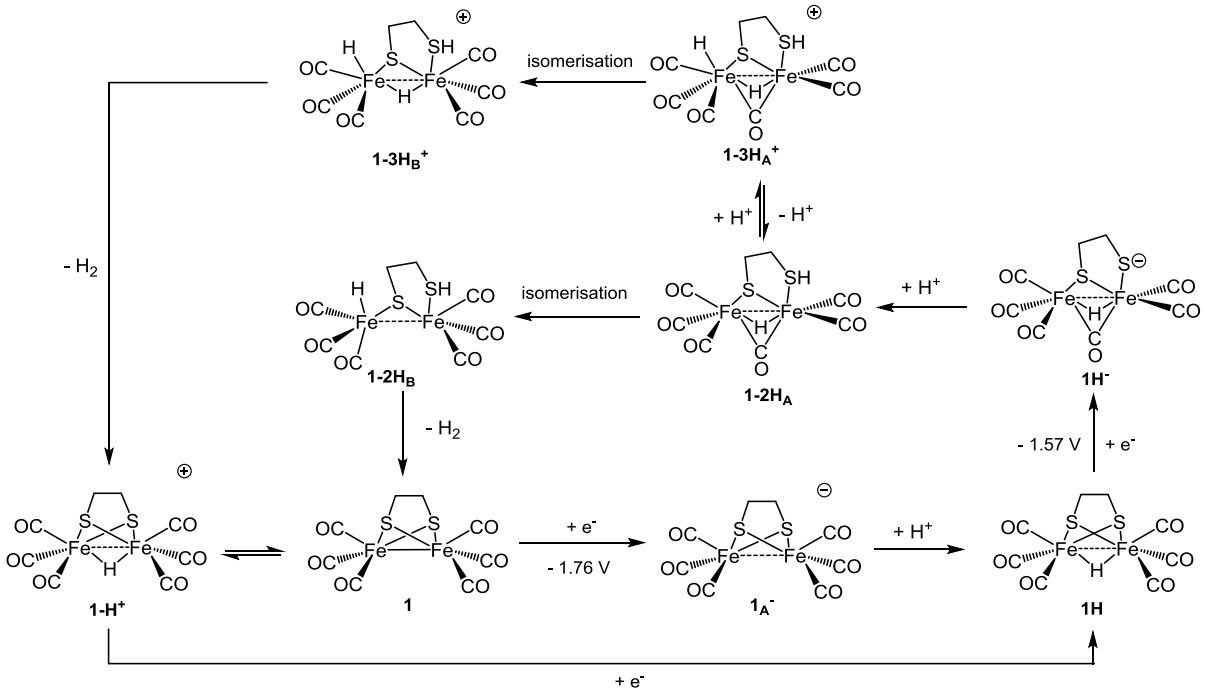

Scheme 5 Proposed proton-reduction processes for **1** (for all complexes apart from **1** the Fe-Fe interaction is given as a dashed line as little is understood about its precise nature)

Reduction of **1** occurs at ca. -1.76 V and the generated anion **1$_A$**$^-$ is readily protonated to give **1H**. This in turn is readily reduced at a potential (-1.57 V) lower than that of the reduction

potential of **1** to afford $\mathbf{1H^+}$. The second reduction leads to major structural changes including scission of an Fe-S bond and trigonal rotation about one $Fe(CO)_3$ moiety leading to formation of a bridging carbonyl. The generated thiolate anion is basic and readily protonates to give $\mathbf{1\text{-}2H_A}$ which contains hydridic and acidic protons. This cannot, however, eliminate hydrogen as the spacial distribution of the two protons is not optimal and a series of rearrangements proceeding via inversion at sulfur and hydride migration to a terminal position generate isomer $\mathbf{1\text{-}2H_B}$ from which a feasible route to hydrogen elimination is possible and **1** is regenerated. A second pathway is also accessible resulting from the further protonation of $\mathbf{1\text{-}2H_A}$ to yield $\mathbf{1\text{-}3H_A^+}$ which after isomerisation and hydrogen loss affords $\mathbf{1\text{-}H^+}$. In all but the strongest acids the equilibrium between this cationic hydride and **1** will lie towards the latter, thus regenerating it for further catalytic cycles.

Complexes **2-7** all facilitate catalytic proton-reduction in MeCN when $HBF_4.Et_2O$ is used as the proton source (Fig. S3). For **2-4** proton-reduction occurs at the first reduction potential consistent with initial formation of a 35-electron anion, which presumably protonates to afford **2-4H** analogous to **1H** (Scheme 5). Following this, further steps cannot be unambiguously determined but given that the diiron centre in **2-4** is not very basic and each has an $Fe(CO)_3$ moiety able to undergo a trigonal rotation then a similar process to that proposed for **1** seems reasonable. For **5** there are clearly two potentials at which H_2 is generated, the first reduction potential of the complex at ca. -2.1 V and a second smaller wave at ca. -1.7 V which we associate with the one electron reduction of $\mathbf{5H^+}$. Thus both channel through the putative 35-electron complex **5H**. A major difference between this and **1-4H** is that lack of a rotatable $Fe(CO)_3$ unit and hence a similar process to that discerned for **1** seems unlikely. This may also explain the instability of **5** in the catalytic system as the electrode was rapidly deposited with an insoluble film resulting from complex decomposition. For **6-7** spectra are of poor quality and little can be discerned regarding the catalytic process except to say that there is some evidence that they follow a similar process to **5** but reduced intermediates appear to be even less stable. Thus overall the proton-reduction behaviour of **2-7** is disappointing and given that it occurs at a higher potential than for **1** they are sadly not worth further study in this respect.

Conclusions

We have successfully prepared and crystallographically characterised a series of ethanedithiolate complexes $[Fe_2(CO)_5(EPh_3)(\mu\text{-edt})]$ (**2-4**) and $[Fe_2(CO)_4(EPh_3)_2(\mu\text{-edt})]$ (**4-7**) (E = P, As, Sb) and this has allowed a comparison of their chemical and electrochemical properties. In all the EPh_3 ligands lie in apical sites, *trans* to the Fe-Fe bond, a common feature in complexes of this type. Substitution significantly alters the barrier to trigonal rotation of the $Fe(CO)_2(EPh_3)$ moiety, such that at accessible temperatures the EPh_3 ligand is also fixed in an apical site in solution, although the trigonal rotation of the $Fe(CO)_3$ units in **2-4** are relatively unperturbed. This likely has important implications to their electrochemistry since a key feature of the reductive chemistry of $[Fe_2(CO)_6(\mu\text{-edt})]$ (**1**) is trigonal rotation upon one-electron reduction leading to a new isomer with a bridging carbonyl that can undergo potential inversion. For the disubstituted complexes **5-7** no evidence of potential inversion was found, consistent with the inability of the respective 35-electron anions to undergo trigonal rotation. For mono-substituted complexes **2-3** (L = PPh_3, $AsPh_3$) a quasi-reversible one-electron reduction is observed and we could find no evidence of potential inversion. For **4** (L = $SbPh_3$) potential inversion was seen leading to a two-electron reduction. At this point we unable to unambiguously determine whether potential inversion results from a similar process as calculated for **1** (Scheme 1) [**17**] or whether it results from loss of the relatively weakly bound $SbPh_3$. While **2-7** are all catalytic for the reduction of $HBF_4.Et_2O$ in MeCN, their performance as compared to many other [FeFe]-hydrogenase biomimics is poor. At the outset of this work we were somewhat surprised, given the vast amount of research on diiron dithiolate complexes carried out over the past five decades [**43**], that complexes with heavy group 15 substituents were virtually unexplored [**26**] and the ease of synthesis and good stability of $AsPh_3$ and $SbPh_3$ derivatives of **1** suggests that this may still be an area which should be examined in further depth.

Experimental section

General considerations. Unless otherwise noted, all the reactions were carried out under a nitrogen atmosphere using standard Schlenk techniques. Reagent-grade solvents were dried using appropriate drying agents and distilled prior to use by standard methods. Infrared spectra were recorded on a Shimadzu FTIR 8101 spectrophotometer. NMR spectra were

recorded on a Bruker DPX 400 instrument. Mass spectra were recorded on a Varian Mat 312 mass spectrometer. Elemental analyses were performed by Microanalytical Laboratories, University College London. The diiron complex $[Fe_2(CO)_6(\mu\text{-edt})]$ (**1**) [**27**] was prepared by literature methods.

Synthesis of $[Fe_2(CO)_5(PPh_3)(\mu\text{-edt})]$ (2): PPh_3 (0.702 g, 2.68 mmol) was added to a toluene solution (20 mL) of **1** (0.50 g, 1.34 mmol) and the mixture was refluxed for 5 h. The resulting solution was cooled and the solvent removed *via* rotary evaporation giving a rust powder which was washed with hexanes and dried. The components of the product mixture were then separated using column chromatography with silica gel using a 1:3 mixture of CH_2Cl_2/hexane as eluent. Three bands were present, the product being the second red band. It was recrystallised upon dissolving in CH_2Cl_2 and layering with hexanes, which when left overnight, afforded dark-red diamond shaped crystals of $[Fe_2(CO)_5(PPh_3)(\mu\text{-edt})]$ (**2**) (182 mg, 59 %). IR (ν(CO); CH_2Cl_2): 2048vs, 1988vs, 1935m cm^{-1}. $^{31}P\{^1H\}$ NMR: ($CDCl_3$): δ 63.5 ppm. ^1H NMR ($CDCl_3$): δ 7.47 (m, 9H), 7.60 (m, 6H), 1.14 (m, 2H), 1.88 (m 2H); $^{13}C\{^1H\}$ NMR (CD_2Cl_2); (298 K) 215.18 (d, J 13.5, 2CO), 210.4 (brs, 3CO), 135.81 (d, J 39.7), 133.10 (d, J 11.3), 130.21 (d, J 1.7), 128.58 (d, J 9.6), 34.92 (s) ppm; (223 K) 215.48 (d, J 8.0, 2CO), 212.71 (s, 2CO), 206.50 (s, CO), 135.61 (d, J 39.9), 133.12 (d, J 11.4), 130.40 (s), 128.79 (d, J 9.5), 34.87 (s) ppm; Anal. calc. for $Fe_2S_2P_1O_5C_{25}H_{19}$: C, 49.50, H, 3.14; Found C, 49.26, H, 3.12.

Synthesis of $[Fe_2(CO)_5(AsPh_3)(\mu\text{-edt})]$ (3): An MeCN solution (20 mL) of **1** (50 mg, 0.13 mmol), $AsPh_3$ (42 mg, 0.14 mmol) and Me_3NO (10 mg, 0.13 mmol) was heated to reflux for 2 h. The solvent was removed under reduced pressure and the residue was chromatographed by TLC on silica gel. Elution with hexane developed two bands. The faster moving band gave unreacted **1**, while the slower moving band afforded $[Fe_2(CO)_5(AsPh_3)(\mu\text{-edt})]$ (**3**) (42 mg, 48 %) as red crystals after recrystallization from hexane/CH_2Cl_2 at 4 °C. IR (υ_{CO}, CH_2Cl_2): 2049vs, 1985vs, 1933m cm^{-1}.^1H NMR ($CDCl_3$): δ 7.53 (m, 6H), 7.43 (m, 9H), 1.92 (m, 2H), 1.32 (m, 2H); Anal. calc. for $Fe_2S_2PAs_1O_5C_{25}H_{19}$: C, 46.15, H, 2.92; Found C, 46.02, H, 2.86.

Synthesis of $[Fe_2(CO)_5(SbPh_3)(\mu\text{-edt})]$ (4): To an MeCN solution (20 mL) of $[Fe_2(CO)_6(\mu\text{-edt})]$ (50 mg, 0.13 mmol) was added $SbPh_3$ (48 mg, 0.14 mmol) and Me_3NO (10 mg, 0.13

mmol) and the reaction mixture was then heated to reflux for 2 h. A similar chromatographic separation and workup described as above gave $[Fe_2(CO)_5(SbPh_3)(\mu\text{-edt})]$ (**4**) (48 mg, 53 %) as red crystals after recrystallization from hexane/CH_2Cl_2 at 4 °C. IR (υ_{CO}, CH_2Cl_2): 2050vs, 1986vs, 1933m cm^{-1}.^{1}H NMR ($CDCl_3$): δ 7.56 (m, 6H), 7.45 (m, 9H), 2.03 (m, 2H), 1.66 (m, 2H); Anal. calc. for $Fe_2S_2Sb_1O_5C_{25}H_{19}$: C, 43.06, H, 2.73; Found C**,** 42.85, H, 2.63.

Synthesis of $[Fe_2(CO)_4(PPh_3)_2(\mu\text{-edt})]$ (5): An MeCN solution (40 mL) of **1** (100 mg, 0.269 mmol), PPh_3 (280 mg, 1.076 mmol) and $Me_3NO.2H_2O$ (119 mg, 1.07 mmol) was stirred and refluxed for 3 h. Solvent was removed and the solid was absorbed into silica from CH_2Cl_2 and eluted with hexane/CH_2Cl_2 (3:1) using flash silica gel column chromatography. Elution with CH_2Cl_2 gives the product from the column, which can be recrystallised from CH_2Cl_2 layered over with hexane to afford very dark-red crystals of **5** (170 mg, 68%). A second crop of crystals can be obtained from the mother solution. IR (υ_{CO}, CH_2Cl_2): 1999vs, 1952m, 1935s cm^{-1}; ^{1}H NMR ($CDCl_3$): δ 7.56 (m, 12H), 7.37 (m, 18H), 0.62 (s, 4H); $^{31}P\{^1H\}$ NMR ($CDCl_3$): 61.3 (s) ppm; Anal. calc. for $Fe_2S_2P_2O_4C_{42}H_{34}$: C, 59.68, H, 3.98; Found C, 60.02, H, 4.08.

Synthesis of $[Fe_2(CO)_4(AsPh_3)_2(\mu\text{-edt})]$ (6): An MeCN solution (25 mL) of **1** (50 mg, 0.134 mmol), $AsPh_3$ (164 mg, 0.536 mmol) and $Me_3NO.2H_2O$ (58 mg, 0.53 mmol) was vigorously stirred and refluxed for 4 h. The solvent was removed and the solid was dried and then redissolved in a minimum amount of CH_2Cl_2 and absorbed onto silica. Flash column chromatography afforded a trace of **1** with hexanes. Elution with diethyl ether afforded two bands the second being collected and identified as **6**. Recrystallization from CH_2Cl_2 and hexanes afforded dark-red platelet crystals of **6** (87 mg, 70%). IR (υ_{CO}, CH_2Cl_2): 1999vs, 1954m, 1935s cm^{-1}; ^{1}H NMR ($CDCl_3$): δ 7.53 (m, 12H), 7.38 (m, 18H), 0.90 (s, 4H); $^{13}C\{^1H\}$ NMR ($CDCl_3$): δ 215.4, 137.4, 133.8, 132.7, 129.7, 128.9, 128.7, 128.5, 33.3; Anal. calc. for $Fe_2S_2As_2O_4C_{42}H_{34}$: C, 53.48, H, 3.53; Found C, 54.34, H, 3.69.

Synthesis of $[Fe_2(CO)_4(SbPh_3)_2(\mu\text{-edt})]$ (7): An MeCN solution (40 mL) of **1** (100 mg, 0.27 mmol), $SbPh_3$ (379 mg, 1.076 mmol) and $Me_3NO.2H_2O$ (119 mg, 1.07 mmol) was stirred and refluxed for 4 h. Work-up and chromatography as described above gave **7** as a red crystalline solid (201 mg, 73%). IR (υ_{CO}, CH_2Cl_2): 1999vs, 1956m, 1937s cm^{-1}; ^{1}H NMR ($CDCl_3$): δ 7.57 (m, 12H), 7.41 (m, 18H), 1.36 (s, 4H); $^{13}C\{^1H\}$ NMR ($CDCl_3$): δ 215.2, 136.3, 135.1,

134.2, 133.7, 129.9, 129.6, 129.3, 128.9, 128.6, 35.3; Anal. calc. for $Fe_2S_2Sb_2O_4C_{42}H_{34}$: C, 49.12, H, 3.41; Found C, 49.36, H, 3.35.

Electrochemistry. Electrochemical measurements were made using a μ-Autolab III potentiostat. CVs were recorded in MeCN with 0.1 M $[Bu_4N][PF_6]$ in a conventional three-electrode cell under an argon or CO atmosphere and are referenced to the Fc/Fc^+ couple. A glassy carbon electrode (3.0 mm diameter) was used as the working electrode, polished on a wet felt polishing pad with alumina gel and dried before each experiment. The counter electrode was a platinum wire and the quasi-reference electrode was a solid silver wire (both ~ 1.0 mm diameter).

X-ray crystallography. Single crystals of **2-7** suitable for X-ray diffraction were grown by slow diffusion of hexane into a dichloromethane solution at 4 °C. All geometric and crystallographic data were collected at 150 K on a Bruker SMART APEX CCD diffractometer using Mo-Kα radiation (λ = 0.71073 Å). Data reduction and integration was carried out with SAINT+ [**44]** and absorption corrections were applied using the program SADABS. Structures were solved by direct methods and developed using alternating cycles of least-squares refinement and difference-Fourier synthesis. All non-hydrogen atoms were refined anisotropically. For **2** hydrogen atoms were located in diffrenece maps and refined independently, for **3-4** hydrogen atoms were placed in the calculated positions and their thermal parameters linked to those of the atoms to which they were attached (riding model). The SHELXTL PLUS V6.10 program package was used for structure solution and refinement [**45]**. Final difference maps did not show any residual electron density of stereochemical significance. The details of the data collection and structure refinement are given in Table 2 and a full list of bond lengths and angles are given in Tables S1-6 respectively. Crystallographic data for the structural analyses have been deposited with the Cambridge Crystallographic Data Center, CCDC Nos. 1947948-952 for **2-7** sequentially and this information can be obtained free of charge from the Cambridge Crystallographic Data Base.

Acknowledgements

We thank King's College London (GO) and the Commonwealth Scholarship Commission (SG) for the provision of PhD studentships.

References

1. J.W. Peters, W.N. Lanzilotta, B.J. Lemon, L.C. Seefeldt, *Science* **1998**, *282*, 1853-1858.
2. Y. Nicolet, C. Piras, P. Legrand, C.E. Hatchikian, J.C. Fontecilla-Camps, *Structure* **1999**, *7*, 13-23.
3. J.C. Gordon, G.J. Kubas, *Organometallics* **2010**, *29*, 4682-4701.
4. T.R. Simmons, G. Berggren, M. Bacchi, M. Fontecave, V. Artero, *Coord. Chem. Rev.* **2014**, *270-271*, 127-150.
5. M. Bruschi, G. Zampella, P. Fantucci, L. De Gioia, *Coord. Chem. Rev.* **2005**, *249*, 1620.
6. C. Tard, C.J. Pickett, *Chem. Rev.* **2009**, *109*, 2245-2274.
7. X. Liu, S.K. Ibrahim, C. Tard, C.J. Pickett, *Coord. Chem. Rev.* **2005**, *249*, 1641-1652.
8. M. Wang, L. Chen, X. Li, L. Sun, *Dalton Trans.* **2011**, *40*, 12793-12800.
9. J.-F. Capon, F. Gloaguen, F.Y. Pétillon, P. Schollhammer, J. Talarmin, *Coord. Chem. Rev.* **2009**, *253*, 1476-1494.
10. M.Y. Darensbourg, E.J. Lyon, J.J. Smee, *Coord. Chem. Rev.* **2000**, *206-207*, 533-561.
11. J.-F. Capon, F. Gloaguen, P. Schollhammer, J. Talarmin, *Coord. Chem. Rev.* **2005**, *249*, 1664-1676.
12. F. Gloaguen, T.B. Rauchfuss, *Chem. Soc. Rev.* **2009**, *38*, 100-108.
13. N. Wang, M. Wang, L. Chen, L. Sun, *Dalton Trans.* **2013**, *42*, 12059-12071.
14. J.-F. Capon, F. Gloaguen, F.Y. Pétillon, P. Schollhammer, J. Talarmin, *Eur. J. Inorg. Chem.* **2008**, 4671-4681.
15. S.P. Best, S.J. Borg, J.M. White, M. Razavet, C.J. Pickett, *Chem. Commun*. **2007**, 4348-4350.
16. I. Aguirre de Carcer, A. DiPasquale, A.L. Rheingold, D.M. Heinekey, *Inorg. Chem.* **2006**, *45*, 8000-8002.
17. G.A.N. Felton, B. Petro, R.S. Glass, D.L. Lichtenberger, D.H. Evans, *J. Am. Chem. Soc*. **2009**, *131*, 11290-11291.
18. E.S. Donovan, G.S. Nichol, G.A.N. Felton, *J. Organomet. Chem.* **2013**, *726*, 9-13.
19. S.J. Borg, J.W. Tye, M.B. Hall, S.P. Best, *Inorg. Chem*. **2007**, *46*, 384-394.
20. E.J. Lyon, I.P. Georgakaki, J.H. Reibenspies, M.Y. Darensbourg, *J. Am. Chem. Soc*. **2001**, *123*, 3268-3278.

21. D. Chong, I.P. Georgakaki, R. Mejia-Rodriguez, J. Sanabria-Chinchilla, M.P. Soriaga, M.Y. Darensbourg, *Dalton Trans*. **2003**, 4158-4163.
22. S.J. Borg, T. Behrsing, S.P. Best, M. Razavet, X. Liu, C.J. Pickett, *J. Am. Chem. Soc*. **2004**, *126*, 16988-16999.
23. R. Mejia-Rodriguez, D. Chong, J.H. Reibenspies, M.P. Soriaga, M.Y. Darensbourg, *J. Am. Chem. Soc.* **2004**, *126*, 12004-12014.
24. S.L. Matthews, D.M. Heinekey, *Inorg. Chem*. **2010**, *49*, 9746-9748.
25. (a) P.C. Ellgen, J.N. Gerlach, *Inorg. Chem*. **1973**, *12*, 2526-2532; (b) R.J. Haines, J.A. De Beer, R. Greatrex, J. *Chem. Soc., Dalton Trans*. **1976**, 1749-1757; (c) J.A. De Beer, R.J. Haines, R. Greatrex, N.N. Greenwood, *J. Chem. Soc. A* **1971**, 3271-3282.
26. (a) W. Gao, T.-T. Zhang, Y.-J. Sun, *Asian J. Chem*. **2014**, *26*, 6687-6688; (b) N.H. Kagalwala, N. Lalaoui, Q.-L. Li, L. Liu, T. Woods, T.B. Rauchfuss, *Inorg. Chem*. **2019**, *58*, 2761-2769.
27. J. Messelhäuser, I.-P. Lorenz, K. Haug, W. Hiller, *Z. Naturforsch.* **1985**, *40B*, 1064-1067.
28. D.L. Hughes, G.J. Leigh, D.R. Paulson, *Inorg. Chim. Acta* **1986**, *120*, 191-195.
29. P. Li, M. Wang, C. He, G. Li, X. Liu, C. Chen, B. Akermark, L. Sun, *Eur. J. Inorg. Chem*. **2005**, 2506-2513.
30. M.C. Ortega-Alfaro, N. Hernández, I. Cerna, J.G. López-Cortés, E. Gómez, R.A. Toscano, C. Alvarez-Toledano, *J. Organomet. Chem*. **2004**, *689*, 885-893.
31. B.-S. Yin, T.-B. Li, M.-S. Yang, *Acta Cryst*. **2011**, *E67*, m1502.
32. A. Jablonskyté, J.A. Wright, C.J. Pickett, *Dalton Trans*. **2010**, *39*, 3026-3034.
33. (a) X.-C. Chen, X.-F. Liu, Z.-Q. Jiang, Y.-X. Zhang, X. Li, X.-N. Tian, X.-H. Liu, *J. Coord. Chem.* **2016**, *69*, 1439-1446; (b) X.-F. Liu, X.-Y. Yu, *Acta Cryst*. **2011**, *E67*, m1552; (c) X.-F. Liu, *Polyhedron* **2016**, *117*, 672-678; (d) X.-F. Liu, Z.-Q. Jiang, Z.-J. Jia, *Polyhedron* **2012**, *33*, 166-170; (e) X.-F. Liu, *J. Coord. Chem.* 70 (2017) 116; (f) X.-F. Liu, *Polyhedron* **2016**, *119*, 71-76.
34. (a) C.-G. Li, Y. Zhu, F. Xue, M.-J. Cui, J.-Y. Shang, *J. Coord. Chem*. **2015**, *68*, 2361-2368; (b) X.-F. Liu, *Trans. Met. Chem*. **2016**, *41*, 547-554.
35. P. Li, M. Wang, C. He, X. Liu, K. Jin, L. Sun, *Eur. J. Inorg. Chem*. **2007**, 3718-3727.
36. (a) T. Liu, B. Li, M.B. Hall, M.Y. Darensbourg, *J. Am. Chem. Soc*. **2009**, *131*, 8296-8307; (b) I.P. Georgakaki, L.M. Thomson, E.J. Lyon, M.B. Hall, M.Y. Darensbourg, *Coord. Chem. Rev*. **2003**, *238-239*, 255-266; (c) B. Li, M. Liu, M.L. Singleton, M.Y. Darensbourg, *Inorg. Chem*. **2009**, *48*, 8393-8403.

37. (a) A. Jablonskyté, L.R. Webster, T.R. Simmons, J.A. Wright, C.J. Pickett, *J. Am. Chem. Soc.* **2014**, *136*, 13038-13044; (b) C. Greco, P. Fantucci, L. De Gioia, R. Suarez-Bertoa, M. Bruschi, J. Talarmin, P. Schollhammer, *Dalton Trans*. **2010**, *39*, 7320-7329; (c) X. Zhao, I.P. Georgakaki, M.L. Miller, J.C. Yarborough, M.Y. Darensbourg, *J. Am. Chem. Soc.* **2001**, *123*, 9710-9711.

38. (a) S. Ezzaher, J.-F. Capon, F. Gloaguen, F.Y. Pétillon, P. Schollhammer, J. Talarmin, *Inorg. Chem*. **2007**, *46*, 3426-3428; (b) J.A. Wright, C.J. Pickett, *Chem. Commun*. **2009**, 5719-5721; (c) X. Zhou, Y.-M. Hsiao, C.-H. Lai, J.H. Reibenspies, M.Y. Darensbourg, *Inorg. Chem*. **2001**, *41*, 699-708; (d) X. Zhou, I.P. Georgakaki, M.L. Miller, R. Mejia-Rodriguez, C.-Y. Chaing, M.Y. Darensbourg, *Inorg. Chem*. **2002**, *41*, 3917-3928; (e) D.G. Unwin, S. Ghosh, F. Ridley, M.G. Richmond, K.B. Holt, G. Hogarth, *Dalton Trans*. **2019**, *48*, 6174-6190; (f) S. Ghosh, B.E. Sanchez, I. Richards, M.N. Haque, K.B. Holt, M.G. Richmond, G. Hogarth, *J. Organomet. Chem*. **2016**, *812*, 247-258. (g) S. Ghosh, G. Hogarth, N. Hollingsworth, K.B. Holt, I. Richards, M.G. Richmond, B.E. Sanchez, D. Unwin, *Dalton Trans*. **2013**, *42*, 6775-6792; (h) R. Zaffaroni, T.B. Rauchfuss, D.J. Gray, L. De Gioia, G. Zampella, *J. Am. Chem. Soc*. **2012**, *134*, 19260-19269.

39. G.A.N. Felton, C.A. Mebi, B.J. Petro, A.K. Vannucci, D.H. Evans, R.S. Glass, D.L. Lichtenberger, *J. Organomet. Chem*. **2009**, *694*, 2681-2699.

40. C. Greco, G. Zampella, L. Bertini, M. Bruschi, P. Fantucci, L. De Gioia, *Inorg. Chem*. **2007**, *46*, 108-116.

41. Y.-C. Liu, K.-T. Chu, Y.-L. Huang, C.-H. Hsu, G.-H. Lee, M.-C. Tseng, M.-H. Chaing, *ACS Catalysis* **2016**, *6*, 2559-2576.

42. P. Surawatanawong, J.W. Tye, M.Y. Darensbourg, M.B. Hall, *Dalton Trans*. 39 (2010) 3093-3104.

43. Y. Li, T.B. Rauchfuss, *Chem. Rev*. **2016**, *116*, 7043-7077.

44. SMART and SAINT+ software for CCDC diffractometers, version 6.1, Bruker AXS, Madison, WI, **2000**.

45. G.M. Sheldrick, M. SHELXTL PLUS, version 6.1, Bruker AXS, Madison, WI, **2000**.

Table 1 Selected structural parameters for **1-7** and $[Fe_2(CO)_5(PPh_3)(\mu\text{-pdt})]$ (**2***)

Compound	**1**[27]	**2**	**3**	**4**	**5**	**6**	**7**	**2***[29]
Fe-Fe	2.502(1)	2.5107(4)	2.5010(8)	2.5034(4)	2.5074(5)	2.4858(5)	2.4741(4)	2.5427(6)
Fe-L		2.2382(6)	2.3316(7)	2.4727(3)	2.2427(6)	2.3214(4)	2.4722(4)	2.2566(9)
					2.2264(6)	2.3362(5)	2.4688(3)	
Fe-S(1)	2.340(1)	2.2559(6)	2.252(1)	2.2510(6)	2.2643(6)	2.2597(7)	2.2598(6)	2.2700(9)
	2.228(1)	2.2498(6)	2.259(1)	2.2538(6)	2.2594(6)	2.2654(7)	2.2570(6)	2.2598(9)
Fe-S(2)	2.245(1)	2.2547(7)	2.257(1)	2.2559(6)	2.2617(6)	2.2586(7)	2.2636(6)	2.264(1)
	2.241(1)	2.2593(6)	2.252(1)	2.2535(6)	2.2590(6)	2.2625(7)	2.2640(6)	2.263(1)
Fe-Fe-L		154.58(2)	152.69(3)	151.74(2)	158.10(2)	153.43(2)	154.57(1)	
					154.05(2)	156.38(2)	153.17(1)	
Fe-S(1)-Fe	68.11(4)	67.73(2)	67.33(3)	67.52(2)	67.32(2)	66.64(2)	66.43(2)	
Fe-S(2)-Fe	67.80(4)	67.59(2)	67.38(3)	67.44(2)	67.37(2)	66.71(2)	66.25(2)	

Table 2 Crystallographic data and structure refinement for **2-7**

Compound	**2**	**3**	**4**	**5**	**6**	**7**
empirical formula	$C_{25}H_{19}Fe_2O_5PS_2$	$C_{25}H_{19}Fe_2O_5AsS_2$	$C_{25}H_{19}Fe_2O_5SbS_2$	$C_{42}H_{34}Fe_2O_4P_2S_2$	$C_{42}H_{34}Fe_2O_4As_2S_2$	$C_{42}H_{34}Fe_2O_4Sb_2S_2$
formula weight	606.19	650.14	696.97	840.45	928.35	1022.01
crystal system	monoclinic	monoclinic	triclinic	monoclinic	monoclinic	monoclinic
space group	$P2_1/c$	$P2_1/c$	$P\bar{1}$ bar	$P2_1/n$	$P2_1/n$	$P2_1/n$
a (Å)	9.181(1)	9.250(2)	8.1452(7)	14.861(2)	15.160(2)	15.539(2)
b (Å)	17.214(2)	17.192(3)	9.2822(8)	15.794(2)	15.807(2)	15.977(2)
c (Å)	16.607(2)	16.682(3)	18.572(2)	17.143(2)	17.191(2)	17.311(2)
α (°)	90	90	90.898(1)	90	90	90
β (°)	103.627(2)	102.835(3)	102.835(3)	109.173(2)	109.822(2)	110.419(2)
γ (°)	90	90	99.878(1)	90	90	90
Volume (Å^3)	2550.8(5)	2586.7(8)	1346.1(2)	3800.5(9)	3875.4(8)	4027.8(8)
Z	4	4	2	4	4	4
D_{calc} (Mg m^{-3})	1.579	1.669	1.720	1.469	1.591	1.685
μ (Mo Kα) (mm^{-1})	1.398	2.586	2.247	1.000	2.593	2.177
F(000)	1232	1304	688	1728	1872	2016
crystal size (mm)	0.36 × 0.24 × 0.20	0.18 × 0.16 × 0.08	0.48 × 0.36 × 0.28	0.42 × 0.38 × 0.26	0.26 × 0.18 × 0.08	0.25 × 0.20 × 0.18
θ range (°)	2.57−28.30	2.37−28.27	2.54−28.28	2.56−28.27	1.92−28.26	1.89−28.25
limiting indices	$-12 \le h \ge 12$,	$-12 \le h \ge 12$,	$-10 \le h \ge 10$,	$-18 \le h \ge 18$,	$-19 \le h \ge 19$,	$-20 \le h \ge 20$,
	$-21 \le k \ge 22$,	$-22 \le k \ge 22$,	$-12 \le k \ge 11$,	$-20 \le k \ge 20$,	$-20 \le k \ge 20$,	$-21 \le k \ge 20$,
	$-21 \le l \ge 21$	$-22 \le l \ge 22$	$-24 \le l \ge 24$	$-22 \le l \ge 22$	$-22 \le l \ge 22$	$-22 \le l \ge 22$
reflections collected	20664	21212	10987	31518	32307	33342
independent reflections (R_{int})	5902 (0.0397)	6034 (0.0735)	5855 (0.0182)	8867 (0.0465)	9067 (0.0465)	9290 (0.0257)
max. and min. transmission	0.7673 and 0.6330	0.8198 and 0.6532	0.5718 and 0.4118	0.7811 and 0.6789	0.8194 and 0.5521	0.6954 and 0.6122
data/restraints/parameters	5902 / 0 / 392	6034 / 0 / 392	5855 / 0 / 392	8867 / 0 / 605	9067 / 0 / 605	9290 / 0 / 605
goodness of fit on F^2	0.998	0.917	1.078	0.904	0.928	1.012
final R indices [$I > 2\sigma(I)$]	R_1 = 0.0352,	R_1 = 0.0446	R_1 = 0.0257	R_1 = 0.0327	R_1 = 0.0310	R_1 = 0.0214
	wR_2 = 0.0819	wR_2 = 0.0833	wR_2 = 0.0652	wR_2 = 0.0652	wR_2 = 0.0621	wR_2 = 0.0476
R indices (all data)	R_1 = 0.0493,	R_1 = 0.0855,	R_1 = 0.0281,	R_1 = 0.0513,	R_1 = 0.0490,	R_1 = 0.0279,
	wR_2 = 0.0876	wR_2 = 0.0955	wR_2 = 0.0664	wR_2 = 0.0679	wR_2 = 0.0647	wR_2 = 0.0486
largest peak and hole (e Å^{-3})	0.631 and −0.806	1.073 and −1.034	1.062 and −1.056	0.499 and −0.447	0.569 and −0.526	0.531 and −0.549

Table 3 Peak reduction potentials and normalised peak reduction currents for **2-4** under a CO at different scan rates

2			**3**			**4**			**1**		
v	**$E_{pa}(1)$**	**$i_{pa}(1)$ x10^{-5}**	*v*	**$E_{pa}(1)$**	**$i_{pa}(1)$ x10^{-5}**	*v*	**$E_{pa}(1)$**	**$i_{pa}(1)$ x10^{-5}**	*v*	**$E_{pa}(1)$**	**$i_{pa}(1)$ x10^{-5}**
0.01	-1.77	3.935	*0.01*	-1.64	2.474	*0.01*	-1.62	6.100	*0.01*	-1.70	9.3625
0.02	-1.94	3.260	*0.02*	-1.65	2.384	*0.02*	-1.62	5.669	*0.02*	-1.79	8.099
0.05	-1.88	2.492	*0.05*	-1.65	2.296	*0.05*	-1.63	4.695	*0.05*	-1.81	7.227
0.1	-1.88	3.264	*0.1*	-1.64	2.209	*0.1*	-1.65	-4.767	*0.1*	-1.75	7.449
0.2	-1.87	3.585	*0.2*	-1.66	2.050	*0.2*	-1.65	4.813	*0.2*	-1.76	6.236
0.5	-1.86	3.332	*0.5*	-1.76	2.583	*0.5*	-1.66	3.936	*0.5*	-1.74	5.269
1	-1.91	3.247	*1*	-1.74	2.741	*1*	-1.65	3.509	*1*	-1.75	4.583
2	-1.91	3.404	*2*	-1.78	2.645	*2*	-1.65	3.120	*2*	-1.81	4.151
5	-1.90	3.316	*5*	-1.83	2.337	*5*	-1.67	2.721	*5*	-1.78	4.132
10	-2.04	2.317	*10*	-1.82	2.872	*10*	-1.71	2.500	*10*	-1.84	3.675
20	-2.00	2.474	*20*	-1.89	2.522	*20*	-1.72	2.489	*20*	-1.84	3.433